



OPEN

## Solid state thin electrolyte to overcome transparency-capacity dilemma of transparent supercapacitor

Jongseon Seo, Geonhui Han, Hyejin Kim & Daeseok Lee

For portable and transparent electronic applications, transparent supercapacitor (T-SC) is developed to act as an energy storing device. Because electric and optical characteristics of the supercapacitor are strongly dependent on its thickness, all solid state T-SC was developed based on sensitively controllable fabrication process. We were able to attain an optimum thickness for the T-SC such that it exhibited an excellent transparency as well as capacity. Thus, the transparency-capacity dilemma, that is, the thickness of a T-SC increases with respect to its capacity while it is inversely proportional to its transparency, was solved through our proposed T-SC structure. Consequently, more than 60% transparency and 80% capacitance retention of 1500 charge/discharge cycles were achieved. The overcoming of transparency-capacity dilemma can enhance the T-SC applicability as a core energy storage device.

Since the industrial revolution, many studies have been conducted on eco-friendly energy such as reusable wind, solar power, tidal power, and geothermal power<sup>1–4</sup>. For effectively utilize the energy produced in various methods, studies on energy storage device have been actively conducted<sup>5–7</sup>. These energy storage devices are operated electro-chemical reaction by various ion movement, such as Li-ion, Na-ion, K-ion, and etc.<sup>8–16</sup>. Especially, the Li-ion based energy storage device has been studied the most, and commercialization has also been conducted a lot.

In addition, development of portable and transparent electronic gadgets is being extensively researched worldwide, for industrial applications. In this regard, various transparent electronic devices such as a transparent memory, transparent transistors, and transparent displays have been proposed<sup>17–19</sup>. However, for energy storage, transparent energy storing devices need to be further investigated. They need high optical transmittance, high energy/power density, rapid charge/discharge time, and long-term lifetime; transparent supercapacitors have been proposed as one of the energy storing devices<sup>20–23</sup>.

The thickness of a T-SC increases with respect to its capacity while it is inversely proportional to the transparency. In other words, a thin T-SC is required for attaining an optimum transparency, but a high capacity can be achieved using a thick T-SC (transparency-capacity dilemma). In more detail, the self-discharge phenomenon in a thin electrolyte is responsible for the loss of capacity<sup>24</sup>. Thus, it is important to optimize the thickness of the T-SC to overcome the transparency-capacity dilemma.

To overcome these limitations, we developed an all-solid-state T-SC, which can easily manipulate the thickness based on the deposition time. The all solid-state T-SC can also increase the mechanical reliability, reduce the total weight of the device, and exhibit an excellent stability on integration<sup>25</sup>. Consequently, we achieved the T-SC having a transmittance of 60% for visible light and excellent capacitance retention after 1300 charge/discharge cycles.

### Results and discussion

Figure 1a illustrates the structure of the developed T-SC. Indium tin oxide (ITO) was used as the material for all electrodes to attain transparency. Furthermore, LiCoO<sub>2</sub> was used as a cathode layer to provide Li ions during the charging process, and WO<sub>3</sub> was applied as an anode layer to store the Li ions; LiPON was used as a stable solid-electrolyte materials<sup>26,27</sup>. Figure 1b shows the images of the T-SC obtained through energy dispersive spectroscopy (EDS) elemental mapping and transmission electron microscopy (TEM). The thickness of LiPON was

Department of Electronic Materials Engineering, Kwangwoon University, Seoul 01897, Republic of Korea. email: leeds@kw.ac.kr

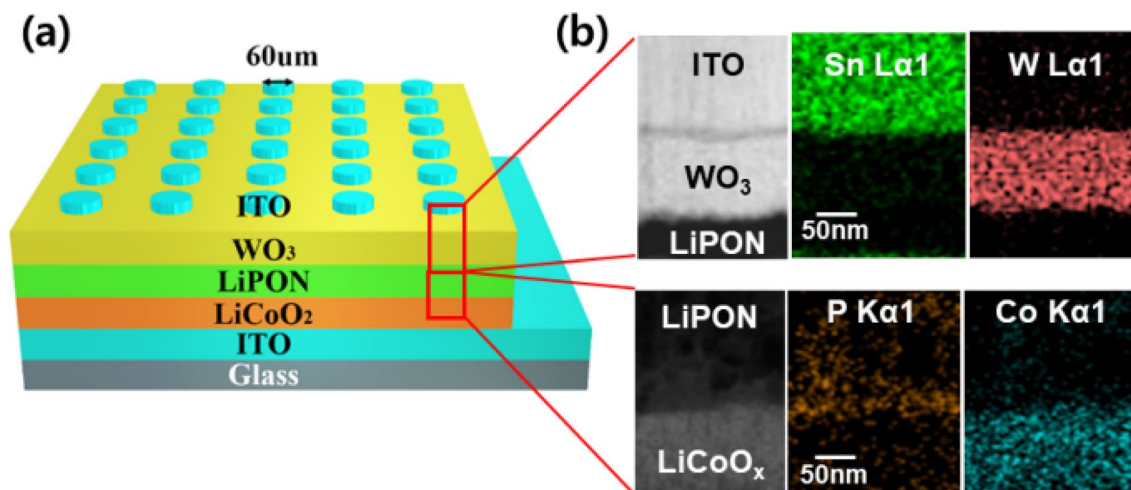


**Figure 1.** (a) Schematics of the developed Glass/ITO/LiCoO<sub>2</sub>/WO<sub>3</sub>/ITO T-SC device. (b) Cross-sectional transmission electron microscopy image of the fabricated T-SC device.

Layer	Sputter process			
	Target	Gas (sccm)	Power (W)	Working pressure (mTorr)
LiCoO <sub>2</sub> (Cathode)	LiCoO <sub>2</sub>	Ar 10	100	8
LiPON (Electrolyte)	Li <sub>3</sub> PO <sub>4</sub>	Ar/N <sub>2</sub> 10/20.5	150	20
WO <sub>3</sub> (Anode)	WO <sub>3</sub>	Ar/O <sub>2</sub> 12/8	150	28.5
ITO (Top electrode)	ITO	Ar 20	100	40

**Table 1.** Optimized T-SC device sputtering process conditions.

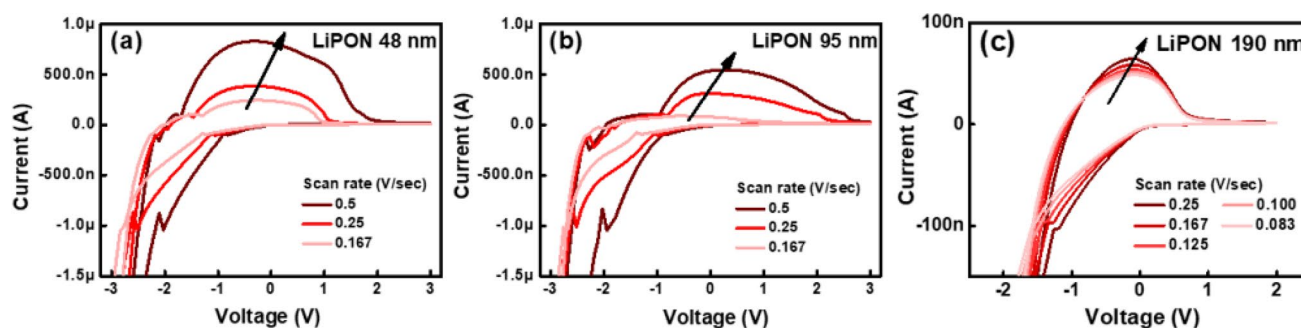
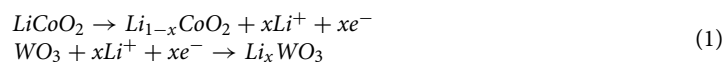


**Figure 2.** Cyclic voltammetry of three devices with LiPON electrolyte thickness of (a) 48 nm, (b) 95 nm, and (c) 190 nm.

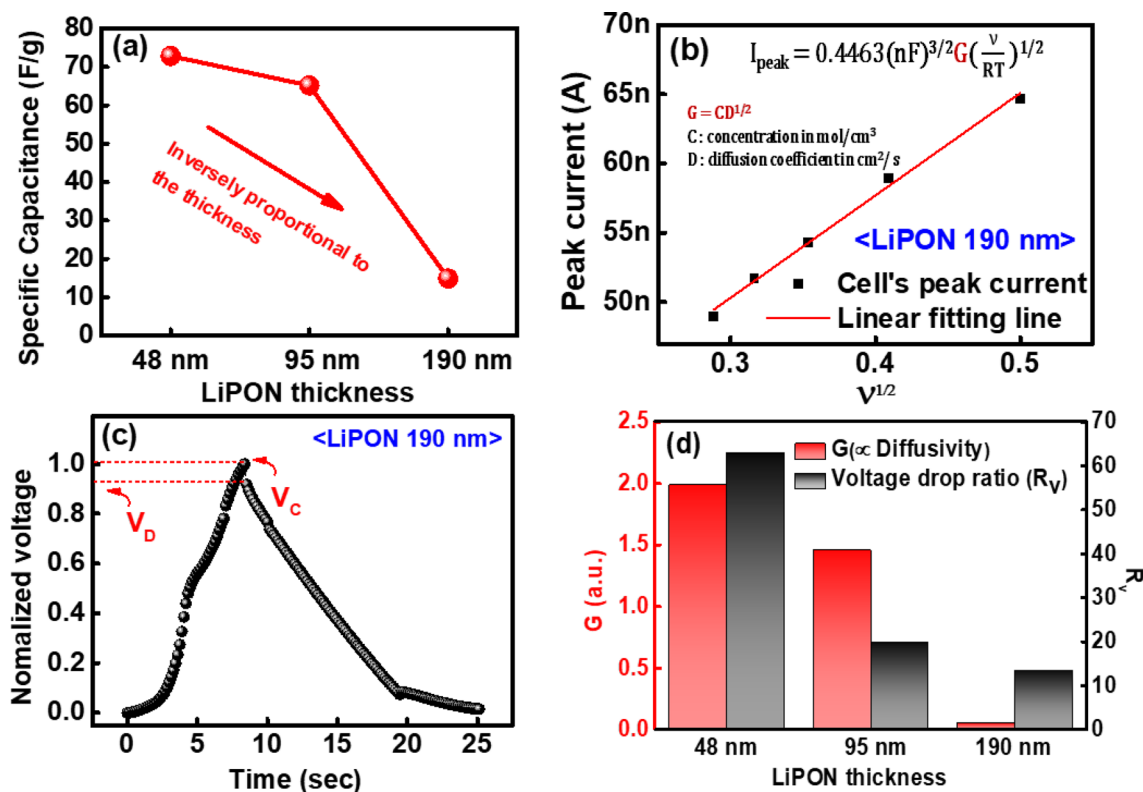
modulated by varying the deposition time. The detailed fabrication process conditions of the optimized device are summarized in “Methods” section and Table 1.

Figure 2a–c show the cyclic voltammetry characteristics for various LiPON thicknesses. These results demonstrate the electrochemical redox reactions between LiCoO<sub>2</sub> and WO<sub>3</sub>. These redox reactions are expressed as follows<sup>28</sup>.



Based on this cyclic voltammetry curve, we calculated the specific capacitance according to the following equation.

$$C_p = \frac{\int IdV}{mv\Delta V} \quad (2)$$



**Figure 3.** (a) Specific capacitance depending on the LiPON thickness. (b) Peak current ( $I_{peak}$ )—scan rate ( $\sqrt{v}$ ) curve for various  $v$ , and (c) galvanostatic charge discharge curve of LiPON 190 nm T-SC device. (d)  $G$  ( $CD^2$ ) and voltage drop ratio ( $R_V$ ) for different LiPON thicknesses.

where  $\int IdV$  is the area under the cyclic voltammetry curve,  $\Delta V$  is the potential window,  $v$  is the scan rate, and  $m$  is the mass of active materials<sup>29</sup>. From the result, we can know that the specific capacitance is inversely proportional to the thickness of LiPON electrolyte layer, as shown in Fig. 3a. Furthermore, we confirmed the movement of Li ions using the Randles–Sevcik equation fitting, as shown in Fig. 3b. The slope of this graph is proportional to  $G$ , which is the product of the concentration ( $C$ ) and the root of diffusivity ( $D^{1/2}$ ). The slope decreases as the thickness of LiPON increases, implying a decrease in diffusivity as well<sup>30</sup>. However, a high diffusivity causes a large amount of desorption of Li ions. As a result, as the LiPON layer became thicker (low diffusivity), the change in peak current ( $I_{peak}$ ) was more stable with the increase in scan rate ( $\sqrt{v}$ ). The results of the cyclic voltammetry curve and the galvanostatic charge-discharge curve depict the stability of the developed T-SC.

Figure 3c presents the galvanostatic charge-discharge characteristics of the LiPON 190 nm T-SC device. We also observed the voltage drop characteristic which are responsible for the reduction in power efficiency and capacity. We defined the voltage drop ratio ( $R_V$ ), to confirm the drop rate at the maximum voltage as follows:

$$\text{Voltage drop ratio}(R_V) = \left[ \frac{V_C - V_D}{V_C} \right] \quad (3)$$

where  $V_C$  and  $V_D$  are the maximum voltages during charging and discharging, respectively (red marked in Fig. 3c). The increase in the desorption of Li ions, owing to a high diffusivity, also increases  $R_V$ . Thus,  $R_V$  is inversely proportional to the thickness of LiPON. Consequently, it can be observed that  $G$  (red bar) and  $R_V$  (black bar) are inversely proportional to the LiPON thickness, as shown in Fig. 3d.

Thus, we optimized the T-SC device with a 190 nm thick LiPON layer that operates most reliably and exhibits the lowest voltage drop ratio. Figure 4a shows the transmittance (60% or more) characteristics of the T-SC device in the visible light band of 400–750 nm. Additionally, the inset photo also depicts its transparent characteristics. According to the power-law relationship, the ratio of the capacitive current ( $k_1 v$ ) to the diffusion current ( $k_2 v^{1/2}$ ) in the total current can be expressed as follows :

$$i(V) = k_1 v + k_2 v^{1/2} \quad (4)$$

where  $i(V)$  is the current response and  $k_1$  and  $k_2$  are constants at different scan rates<sup>31</sup>.

Figure 4b shows that the capacitive current ratio of the T-SC device at a scan rate of 0.083 V/s is 19.7%. The diffusion-controlled and capacitive-controlled contribution percentages for different scan rates are shown in Fig. 4c. The capacitive contribution gradually increases with an increase in the scan rate. Subsequently, it exhibited the highest capacitive current ratio at 0.25 V/s. This indicates the limit of the diffusion process at high scan rates<sup>32</sup>.

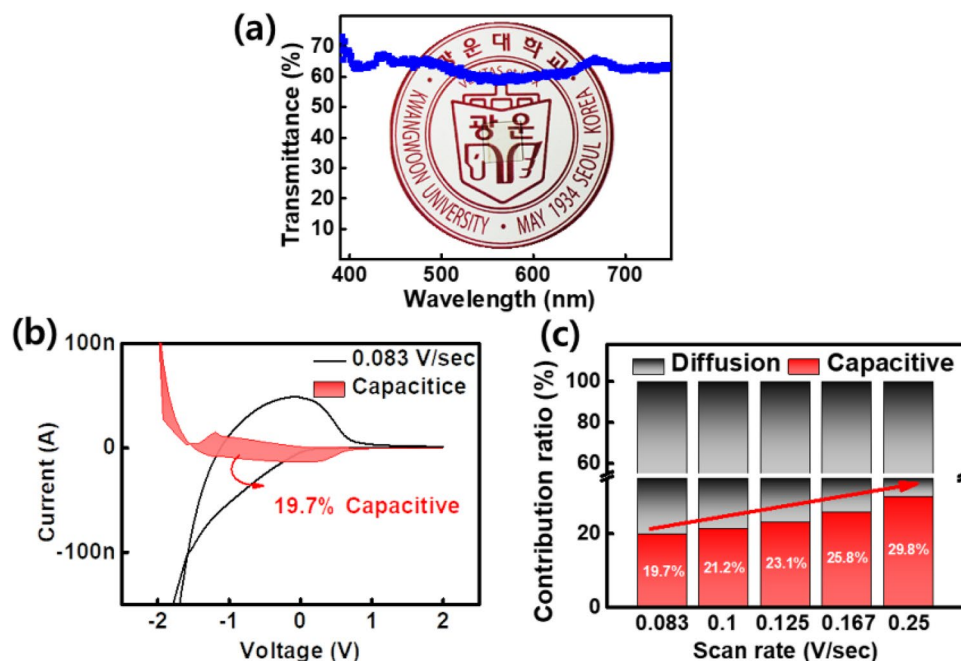


**Figure 4.** (a) Optical transmittance of T-SC device and the corresponding image (inset). (b) Capacitive and diffusion-controlled charge storage process at a scan rate of 0.083 V/s. (c) Contribution ratio of capacitive and diffusion-controlled currents at various scan rates of the T-SC device.

The galvanostatic charge/discharge curve (17.68 mA/cm<sup>2</sup> and 7.072 mA/cm<sup>2</sup> of constant charge/discharge current density for 9 and 16 s, respectively) was approximately triangular with a low voltage drop, as shown in Fig. 5. Moreover, we calculated the coulombic efficiency of the T-SC device based on following equation<sup>33</sup>.

$$\text{Coulombic efficiency} = \frac{Q_{\text{discharge}}}{Q_{\text{charge}}} \times 100(\%) = \frac{I_{\text{discharge}} \times t_{\text{discharge}}}{I_{\text{charge}} \times t_{\text{charge}}} \times 100(\%) \quad (5)$$

where,  $Q_{\text{charge}}$  and  $Q_{\text{discharge}}$  are the amount of charge at charging and discharging,  $I_{\text{charge}}$  and  $I_{\text{discharge}}$  are the charge, discharge constant current, and  $t_{\text{charge}}$ ,  $t_{\text{discharge}}$  are the charge and discharge time, respectively. As a result, the T-SC device has a 71.1% coulombic efficiency. In addition, after 1500 charge/discharge cycles, the T-SC exhibited a very stable capacitance (more than 80% of the original capacitance), indicating a long-term electrochemical stability. This is further confirmed by the inconspicuous change between the charging and discharging curves of the 15th–18th and 1355th–1358th cycles, as shown in Fig. 5b. Furthermore, we calculated specific energy density and power density based on below equations:<sup>29,34–36</sup>

$$E = \frac{1}{2} C_p (\Delta v)^2 \quad P = \frac{E}{\Delta t} \quad (6)$$

where  $E$  is energy density,  $P$  is power density,  $C_p$  is specific capacitance,  $\Delta v$  is the voltage scan range, and  $\Delta t$  is the discharge time. It also exhibited excellent specific energy density of 10.947 Wh/kg and specific power density of 2463.156 W/kg, respectively. From the replotted Ragone plot (fig. 5(c)), the developed device can be considered as the supercapacitor which is located at the intermediate between 2nd cells and capacitor of the Ragone plot.

## Conclusion

We fabricated an all-solid-state T-SC that can be easily optimized and is physically stable. Furthermore, the transparency-capacity dilemma was overcome by controlling the deposition time to regulate the thickness of the electrolyte. Consequently, we fabricated a device with a transmittance of more than 60% transparency in the visible light band. In addition, this device exhibits charge discharge characteristics of up to 1500 cycles and more. It exhibits a high stability during operation with a capacitance retention of at least 80%. Owing to its excellent capacity and transparency characteristics, it is expected to have various applications as a transparent energy storing device.

## Methods

A transparent supercapacitor (ITO/LiCoO<sub>2</sub>/LiPON/WO<sub>3</sub>/ITO) was fabricated on an ITO-coated glass substrate (AMG, Korea). Subsequently, a 100 nm thick layer of LiCoO<sub>2</sub> was deposited to act as the cathode, on the 150 nm thick ITO deposited bottom electrode. We deposited LiCoO<sub>2</sub> layer by using LiCoO<sub>2</sub> target in Ar ambient gas. Sputtering power was 100 W and working pressure was 8 mTorr. Thereafter, a 190 nm thick electrolyte (LiPON) layer was formed by reactive sputtering of a Li<sub>3</sub>PO<sub>4</sub> target in Ar and N<sub>2</sub> mixed ambient gas with sputtering power

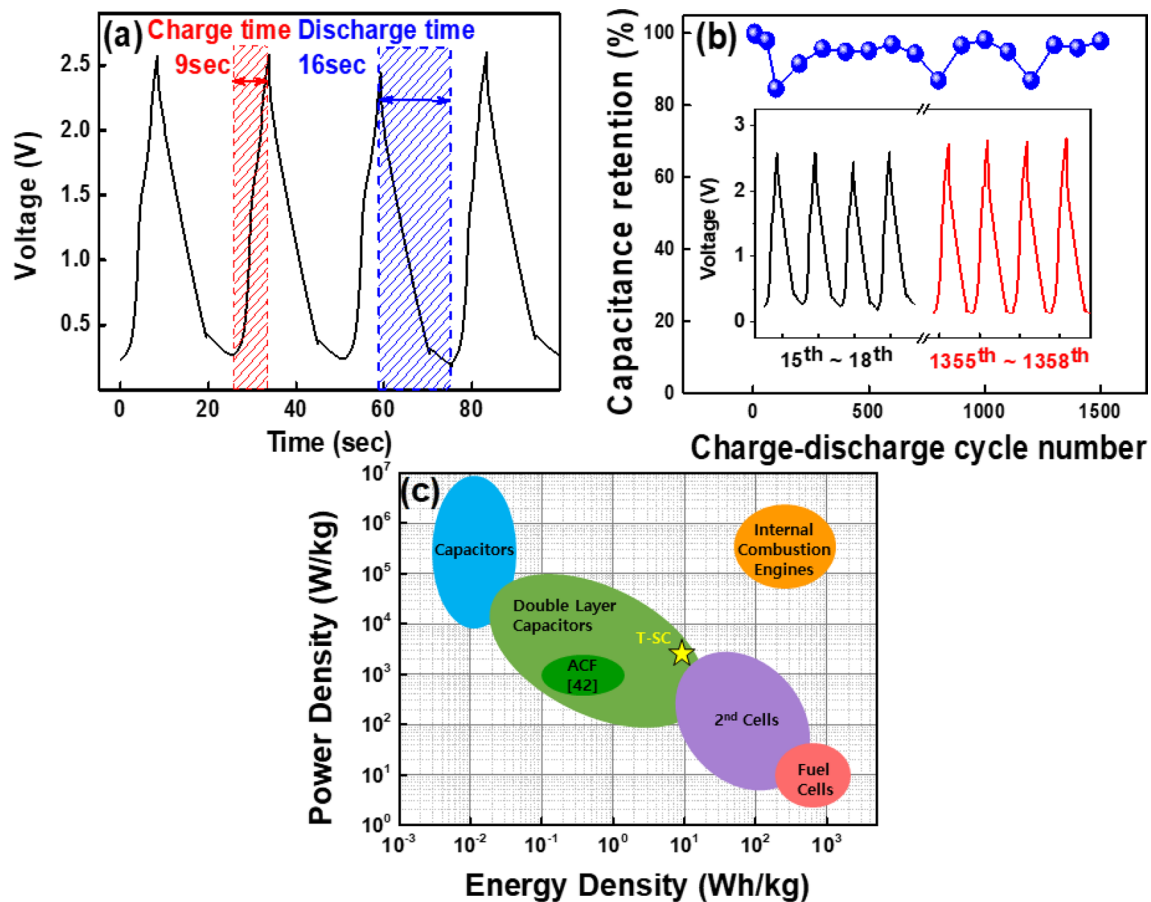


**Figure 5.** (a) Galvanostatic charge discharge curve of the T-SC device. (b) Capacitance retention, which denotes a long-term stability of 1500 cycles. (c) Ragone plot for various energy storage devices (replotted from Ref.<sup>42</sup>). The developed T-SC device (yellow star) exhibits supercapacitor characteristics.

of 150 W at 20 mTorr working pressure. Furthermore, a 100 nm thick ( $\text{WO}_3$ ) layer was deposited to act as the anode. The  $\text{WO}_3$  layer was deposited by utilizing  $\text{WO}_3$  target in Ar and  $\text{O}_2$  mixed ambient gas with sputtering power of 150 W and 28.5 mTorr working pressure. Finally, a 150 nm ITO top electrode was deposited using circular shadow mask with a 60  $\mu\text{m}$  diameter (in Ar ambient gas with 100 W sputtering power and 40 mTorr working pressure).

Unlike previously reported liquid based fabrication processes<sup>37–41</sup>, to sensitively control the thickness of thin film layer, all layers were fabricated by solid state fabrication processes such as a radio frequency sputtering, reactive sputtering, and photo lithography. In addition, to achieve stable fabrication conditions, commercial sputtering targets purchased from the TAEWON SCIENTIFIC CO. LTD. (with 99.9% purity) were utilized. The detailed fabrication process is summarized as shown in Table 1. The electrical analyses were performed using a Keithley 2450 source-meter.

### Data availability

The datasets used and/or analysed during the current study available from the corresponding author on reasonable request.

Received: 27 May 2022; Accepted: 6 September 2022

Published online: 23 September 2022

### References

1. Olabi, A. G., Mahmoud, M., Soudan, B., Wilberforce, T. & Ramadan, M. Geothermal based hybrid energy systems, toward eco-friendly energy approaches. *Renew. Energy* **147**, 2003–2012 (2020).
2. Sharma, A., Srivastava, J., Kar, S. K. & Kumar, A. Wind energy status in India: A short review. *Renew. Sustain. Energy Rev.* **16**, 1157–1164 (2012).
3. Park, J.-I. & Kim, T. Institutional improvement measures for environmental assessment in the pursuit of eco-friendly ocean renewable energy development in South Korea. *Renew. Sustain. Energy Rev.* **58**, 526–536 (2016).
4. Ahmed, S., Jannat, F., Khan, M. A. K. & Alim, M. A. Numerical development of eco-friendly  $\text{Cs}_2\text{TiBr}_6$  based perovskite solar cell with all-inorganic charge transport materials via scaps-1d. *Optik* **225**, 165765 (2021).
5. Kim, M. *et al.* Energy-storing hybrid 3d vertical memory structure. *IEEE Electron Device Lett.* **40**, 1622–1625 (2019).

6. Li, Y. & Lu, J. Metal-air batteries: Will they be the future electrochemical energy storage device of choice?. *ACS Energy Lett.* **2**, 1370–1377 (2017).
7. Divya, K. & Østergaard, J. Battery energy storage technology for power systems-an overview. *Electr. Power Syst. Res.* **79**, 511–520 (2009).
8. Pandit, B., Sougrati, M. T., Fraisse, B. & Monconduit, L. Exploration of a na3v2 (po4) 3/c-pb full cell na-ion prototype. *Nano Energy* **95**, 107010 (2022).
9. Kozen, A. C., Pearse, A. J., Lin, C.-F., Noked, M. & Rubloff, G. W. Atomic layer deposition of the solid electrolyte LiPON. *Chem Mater* **27**, 5324–5331 (2015).
10. Pandit, B., Fraisse, B., Stievano, L., Monconduit, L. & Sougrati, M. T. Carbon-coated fepo4 nanoparticles as stable cathode for na-ion batteries: A promising full cell with a na15pb4 anode. *Electrochimica Acta* **409**, 139997 (2022).
11. Pandit, B. *et al.* High stability and long cycle life of rechargeable sodium-ion battery using manganese oxide cathode: A combined density functional theory (dft) and experimental study. *ACS Appl. Mater. Interfaces* **13**, 11433–11441 (2021).
12. Martínez-Cisneros, C. S. *et al.* Development of sodium hybrid quasi-solid electrolytes based on porous nasicon and ionic liquids. *J. Eur. Ceram. Society* **41**, 7723–7733 (2021).
13. Jamil, M. A. *et al.* Highly efficient tin fluoride nanocomposite with conductive carbon as a high performance anode for li-ion batteries. *J. Alloys Comp.* **900**, 163447 (2022).
14. Choi, G., Lee, J. & Kim, D. Uncovering the structural evolution in na-excess layered cathodes for rational use of an anionic redox reaction. *ACS Appl. Mater. Interfaces* **12**, 29203–29211 (2020).
15. Nitta, N., Wu, F., Lee, J. T. & Yushin, G. Li-ion battery materials: present and future. *Mater. Today* **18**, 252–264 (2015).
16. Kubota, K., Dahbi, M., Hosaka, T., Kumakura, S. & Komaba, S. Towards k-ion and na-ion batteries as “beyond li-ion”. *Chem. Record* **18**, 459–479 (2018).
17. Yang, Y. *et al.* Transparent lithium-ion batteries. *Proc. Natl. Acad. Sci.* **108**, 13013–13018 (2011).
18. Yao, J. *et al.* Highly transparent nonvolatile resistive memory devices from silicon oxide and graphene. *Nat. Commun.* **3**, 1–8 (2012).
19. Gu, G., Bulović, V., Burrows, P., Forrest, S. & Thompson, M. Transparent organic light emitting devices. *Appl. Phys. Lett.* **68**, 2606–2608 (1996).
20. Frackowiak, E. Carbon materials for supercapacitor application. *Phys. Chem. Chem. Phys.* **9**, 1774–1785 (2007).
21. Vangari, M., Pryor, T. & Jiang, L. Supercapacitors: Review of materials and fabrication methods. *J. Energy Eng.* **139**, 72–79 (2013).
22. Chen, Z. *et al.* Multiple-stimuli-responsive and cellulose conductive ionic hydrogel for smart wearable devices and thermal actuators. *ACS Appl. Mater. Interfaces* **13**, 1353–1366 (2020).
23. Ke, Y. *et al.* Emerging thermal-responsive materials and integrated techniques targeting the energy-efficient smart window application. *Adv. Funct. Mater.* **28**, 1800113 (2018).
24. Liu, Y., Chang, J., Liu, L., Kang, L. & Ran, F. Study on the voltage drop of vanadium nitride/carbon composites derived from the pectin/vcl 3 membrane as a supercapacitor anode material. *N. J. Chem.* **44**, 6791–6798 (2020).
25. Huang, J. *et al.* Self-powered integrated system of a strain sensor and flexible all-solid-state supercapacitor by using a high performance ionic organohydrogel. *Mater. Horizons* **7**, 2085–2096 (2020).
26. Xiao, D.-L. *et al.* Improved performance of all-solid-state lithium batteries using lipon electrolyte prepared with li-rich sputtering target. *Solid State Ionics* **324**, 202–206 (2018).
27. Kozen, A. C., Pearse, A. J., Lin, C.-F., Noked, M. & Rubloff, G. W. Atomic layer deposition of the solid electrolyte lipon. *Chem. Mater.* **27**, 5324–5331 (2015).
28. Sasaki, A. *et al.* Durability evaluation of hexagonal wo3 electrode for lithium ion secondary batteries. *Microelectron. Reliability* **68**, 86–90 (2017).
29. Pandit, B. & Sankapal, B. R. Cerium selenide nanoparticle/multiwalled carbon nanotube composite electrodes for solid-state symmetric supercapacitors. *ACS Appl. Nano Mater.* **5**, 3007–3017 (2022).
30. Lee, C. *et al.* Two-terminal structured synaptic device using ionic electrochemical reaction mechanism for neuromorphic system. *IEEE Electron Device Lett.* **40**, 546–549 (2019).
31. Liu, J. *et al.* Advanced energy storage devices: Basic principles, analytical methods, and rational materials design. *Adv. Sci.* **5**, 1700322 (2018).
32. Xie, B. *et al.* Pseudocapacitive co9s8/graphene electrode for high-rate hybrid supercapacitors. *Carbon* **141**, 134–142 (2019).
33. Laheäär, A., Przygocki, P., Abbas, Q. & Béguin, F. Appropriate methods for evaluating the efficiency and capacitive behavior of different types of supercapacitors. *Electrochem. Commun.* **60**, 21–25 (2015).
34. Pandit, B., Agarwal, A., Patel, P. & Sankapal, B. R. The electrochemical kinetics of cerium selenide nano-pebbles: The design of a device-grade symmetric configured wide-potential flexible solid-state supercapacitor. *Nanoscale Adv.* **3**, 1057–1066 (2021).
35. Pandit, B., Rondiya, S. R., Cross, R. W., Dzade, N. Y. & Sankapal, B. R. Vanadium telluride nanoparticles on mwcnts prepared by successive ionic layer adsorption and reaction for solid-state supercapacitor. *Chem. Eng. J.* **429**, 132505 (2022).
36. Pandit, B. *et al.* One-pot hydrothermal preparation of hierarchical manganese oxide nanorods for high-performance symmetric supercapacitors. *J. Energy Chem.* **65**, 116–126 (2022).
37. Pandit, B., Kumar, N., Koinkar, P. M. & Sankapal, B. R. Solution processed nanostructured cerium oxide electrode: Electrochemical engineering towards solid-state symmetric supercapacitor device. *J. Electroanal. Chem.* **839**, 96–107 (2019).
38. Pandit, B., Pande, S. A. & Sankapal, B. R. Facile silar processed bi2s3: Pbs solid solution on mwcnts for high-performance electrochemical supercapacitor. *Chin. J. Chem.* **37**, 1279–1286 (2019).
39. Goda, E. S. *et al.* Al-doped co9s8 encapsulated by nitrogen-doped graphene for solid-state asymmetric supercapacitors. *Chem. Eng. J.* **428**, 132470 (2022).
40. Pande, S. A., Pandit, B. & Sankapal, B. R. Vanadium oxide anchored mwcnts nanostructure for superior symmetric electrochemical supercapacitors. *Mater. Design* **182**, 107972 (2019).
41. Pande, S. A., Pandit, B. & Sankapal, B. R. Facile chemical route for multiwalled carbon nanotube/mercury sulfide nanocomposite: High performance supercapacitive electrode. *J. Colloid Interface Sci.* **514**, 740–749 (2018).
42. Fukuhara, M. *et al.* Amorphous cellulose nanofiber supercapacitors with voltage-charging performance. *Sci. Rep.* **12**, 1–6 (2022).

## Acknowledgements

This work was supported by the National Research Foundation of Korea (NRF) Grant funded by the Korea Government (MSIP) (NRF-2020R1C1C1005925), partially supported by the MSIT (Ministry of Science and ICT), Korea, under the ITRC (Information Technology Research Center) support program (IITP-2022-RS-2022-00156225) supervised by the IITP (Institute for Information & Communications Technology Planning & Evaluation).

## Author contributions

D.S.L. conceived and directed the research. J.S. conducted the experiment. J.S., G.H., and H.J. analysed the results. J.S. wrote the manuscript. All authors reviewed the manuscript.

### Competing interests

The authors declare no competing interests.

### Additional information

**Correspondence** and requests for materials should be addressed to D.L.

**Reprints and permissions information** is available at [www.nature.com/reprints](http://www.nature.com/reprints).

**Publisher's note** Springer Nature remains neutral with regard to jurisdictional claims in published maps and institutional affiliations.



**Open Access** This article is licensed under a Creative Commons Attribution 4.0 International License, which permits use, sharing, adaptation, distribution and reproduction in any medium or format, as long as you give appropriate credit to the original author(s) and the source, provide a link to the Creative Commons licence, and indicate if changes were made. The images or other third party material in this article are included in the article's Creative Commons licence, unless indicated otherwise in a credit line to the material. If material is not included in the article's Creative Commons licence and your intended use is not permitted by statutory regulation or exceeds the permitted use, you will need to obtain permission directly from the copyright holder. To view a copy of this licence, visit <http://creativecommons.org/licenses/by/4.0/>.

© The Author(s) 2022